New astrophysical S factor for the ^{15}N(p, γ)^{16}O reaction via the asymptotic normalization coefficient (ANC) method

A. M. Mukhamedzhanov,[1] P. Bém,[2] V. Burjan,[2] C. A. Gagliardi,[1] V. Z. Goldberg,[1] Z. Hons,[2] M. La Cognata,[3] V. Kroha,[2] J. Mrázek,[2] J. Novák,[2] Š. Piskoř,[2] R. G. Pizzone,[3] A. Plunkett,[1] S. Romano,[3] E. Šimečková,[2] C. Spitaleri,[3] L. Trache,[1] R. E. Tribble,[1] F. Veselý,[2] and J. Vincour[2]

[1]*Cyclotron Institute, Texas A&M University, College Station, Texas 77843, USA*
[2]*Nuclear Physics Institute, Czech Academy of Sciences, 250 68 Řež near Prague, Czech Republic*
[3]*Università di Catania and INFN Laboratori Nazionali del Sud, Catania, Italy*
(Received 8 November 2007; revised manuscript received 27 May 2008; published 22 July 2008)

The ^{15}N(p, γ)^{16}O reaction provides a path from the CN cycle to the CNO bi-cycle and CNO tri-cycle. The measured astrophysical factor for this reaction is dominated by resonant capture through two strong $J^{\pi} = 1^{-}$ resonances at $E_R = 312$ and 962 keV and direct capture to the ground state. Asymptotic normalization coefficients (ANCs) for the ground and seven excited states in ^{16}O were extracted from the comparison of experimental differential cross sections for the ^{15}N(^{3}He,d)^{16}O reaction with distorted-wave Born approximation calculations. Using these ANCs and proton and α resonance widths determined from an R-matrix fit to the data from the ^{15}N(p, α)^{12}C reaction, we carried out an R-matrix calculation to obtain the astrophysical factor for the ^{15}N(p, γ)^{16}O reaction. The results indicate that the direct capture contribution was previously overestimated. We find the astrophysical factor to be $S(0) = 36.0 \pm 6.0$ keV b, which is about a factor of 2 lower than the presently accepted value. We conclude that for every 2200 ± 300 cycles of the main CN cycle one CN catalyst is lost due to this reaction.

I. INTRODUCTION

The ^{15}N(p, γ)^{16}O reaction provides the path to form ^{16}O in stellar hydrogen burning, thus transforming the CN cycle into the CNO bi-cycle and CNO tri-cycle. In stellar environments, the ^{15}N(p, γ)^{16}O reaction proceeds at very low energies, where it is dominated by resonant capture to the ground state through the first two interfering $J^{\pi} = 1^{-}$ s wave resonances at $E_R = 312$ and 964 keV, where E_R is the resonance energy in the center-of-mass (c.m.) system [1,2].

Direct measurements of the ^{15}N(p, γ)^{16}O reaction have been reported by Rolfs and Rodney [1] down to proton energies of $E_p \geqslant 155$ keV and earlier by Hebbard [2] for proton energies down to $E_p \geqslant 220$ keV. These measurements disagree at energies below 300 keV by up to a factor of 2. To fit their low-energy data to obtain an astrophysical S factor, Rolfs and Rodney included the interference of the two 1^{-} resonant capture amplitudes with the nonresonant (direct) component to the ground state of ^{16}O. The direct capture term plays an important role in their analysis and, to fit the data, they allowed the spectroscopic factor (SF) for the ^{15}N $+ p$ configuration in the ^{16}O ground state to vary.

The R-matrix amplitude for the radiative capture reaction is given by the sum of the resonant and nonresonant (direct capture) amplitudes. The channel radius r_0 in the R-matrix method divides the internal and external regions. The direct capture contribution from the internal region ($r < r_0$) is absorbed in the resonance term. The nonresonant capture amplitude is determined by the radial integral taken from the channel radius r_0 to infinity [3]. In the external region $r > r_0$, the bound-state wave function describing the final state can be approximated by its asymptotic term. Hence the nonresonant capture amplitude in the R-matrix approach is

proportional to the proton asymptotic normalization coefficient (ANC).

To better understand the nonresonant capture part of the low-energy astrophysical factor for ^{15}N(p, γ)^{16}O, we measured the ANCs for proton removal from the ground state and seven excited states of ^{16}O. In previous studies [4–6] we have shown that the (^{3}He, d) proton transfer reaction at incident energies of around 10 MeV/nucleon is a reliable tool to determine ANCs. Here we report a measurement of the ANCs using the ^{15}N(^{3}He, d)^{16}O reaction. The ANCs are used to determine, within the R-matrix approach, the direct capture astrophysical S factors to the corresponding eight bound states.

II. EXPERIMENTAL SET UP AND RESULTS

The experiment was performed using a momentum analyzed 25.74 MeV ^{3}He beam from the U-120M cyclotron at the Nuclear Physics Institute of CAS incident on a nitrogen gas target. The target gas chamber contained nitrogen gas enriched to 99.99% ^{15}N. The gas chamber windows were 3.05-μm-thick havar foils. The working pressure was kept between 205 and 208 mbar and was monitored by a gas control system, which registered the pressure and temperature of the gas inside the chamber. Reaction products were observed by a pair of ΔE-E telescopes consisting of 250-μm- and 3-mm-thick Si(Li) surface barrier detectors. Both telescopes were equipped with a pair of collimating slits of dimensions 2×3 mm. The near and far slits were located 80 and 160 mm, respectively, from the center of the target cell. The effective target thickness at each reaction angle was determined by a Monte Carlo simulation using the measured geometry of the system. One telescope was fixed at $20°$ as a monitor and the
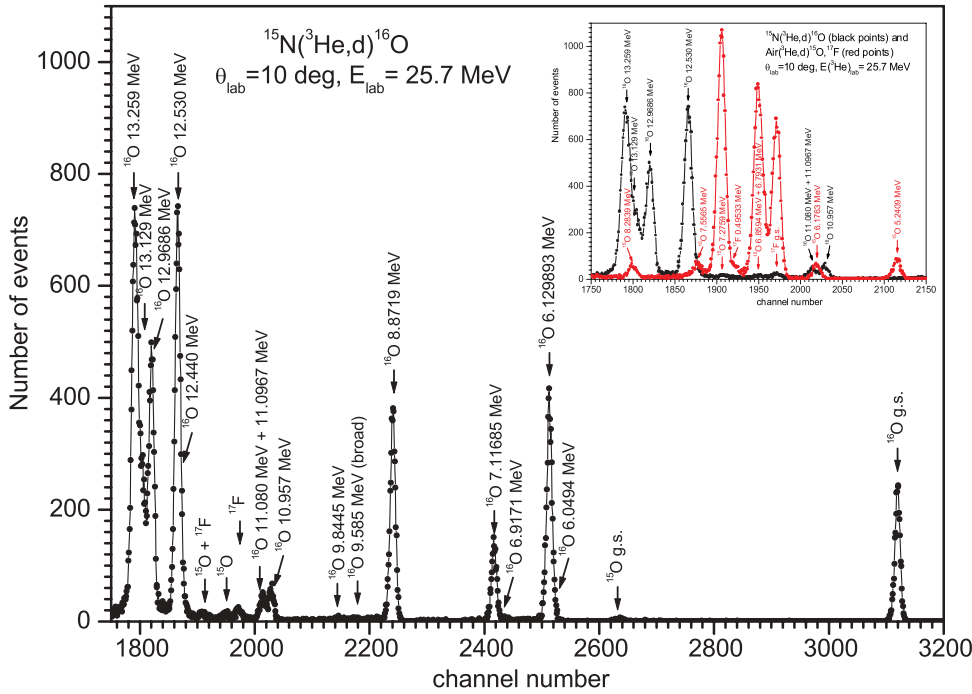
FIG. 1. (Color online) The deuteron spectrum from the ^{15}N(^{3}He, d)^{16}O reaction at $\theta_{\text{lab}} = 10.5°$. The large picture shows the deuteron groups from pure ^{15}N gas. The comparison of deuteron spectra from ^{15}N gas and air (red points) in insert shows that ^{15}N gas contains no admixture of ^{14}N.

second one was moved between laboratory angles of 6.5° and 60° to obtain angular distributions for the reaction. All data, including the integrated charge from the Faraday cup, were collected on-line for later processing.

Several sources contribute to the overall uncertainties in the data points that yield the angular distributions. The uncertainties due to the effective gas target thickness and detector solid angle were about 8%. The integrated charge of the beam was measured with an uncertainty of 3%. This level of uncertainty has been achieved by repeated calibration checks and a determination of the extremely small leakage current in the Faraday cup assembly. These uncertainties together with statistical uncertainties, which were usually less than 5% around the maxima in the angular distributions for the stronger transitions, lead to a total uncertainty at forward angles less than 10% for most transitions.

Angular distributions were obtained for elastic scattering and 14 deuteron groups from the ^{15}N(^{3}He, d)^{16}O reaction populating states below and above the particle emission threshold of ^{16}O, but only 8 deuteron groups corresponding to proton transfer to the bound states in ^{16}O were further analyzed. A typical deuteron spectrum is shown in Fig. 1. We did not observe transitions to the subthreshold state, $J^\pi = 1^-$, $E_x = 9.585$ MeV, which is an $l = 0$ level that could play an important role in both ^{15}N(p, γ)^{16}O and ^{15}N(p, α)^{12}C due to the absence of the centrifugal barrier in the entry channel. There is contradictory information about the proton spectroscopic factor for this level [7]. Our data indicate that the SF factor is too low to allow the state to be observed in the transfer reaction.

III. OPTICAL MODEL POTENTIALS AND DWBA CALCULATIONS

An optical model analysis was carried out to extract spectroscopic information from the angular distributions.

DWBA calculations using DWUCK5 [8] were performed with entrance channel optical model parameter sets that were deduced from fits to the elastic scattering data. The form of the phenomenological optical potential that we used was

$$U(r) = V_c(r) - Vf(x_o) + \left(\frac{\hbar}{m_\pi.c}\right)^2 V_{\text{so}}(\boldsymbol{\sigma \cdot l})\frac{1}{r}\frac{d}{dr}f(x_{\text{so}})$$
$$- i\left[Wf(x_w) - 4W_d\frac{d}{dr}f(x_d)\right], \quad (1)$$

where $f(x_i) = (1 + e^{x_i})^{-1}$ and $x_i = (r - r_i A^{1/3})/a_i$ represents the usual Woods-Saxon form factor. V, W, W_d, and V_{so} are the real, imaginary volume, imaginary surface, and spin-orbital potential depths, respectively, with appropriate radii r_i and diffusenesses a_i, and $V_c(r)$ is the Coulomb potential of a uniformly charged spherical nucleus of a radius $r_{\text{coul}} = r_c A^{1/3}$ (A is the mass number of target nucleus).

A search for the optical model parameters in the entrance channel was done fitting the elastic-scattering data with the computer code ECIS79 [9]. We used two different sets of optical model parameters as seed parameters to include potentials with surface absorption [10] and volume absorption [11] (see Table I). We did not include a spin-orbit coupling term in the seed potentials. When fitting the optical model parameters (V, a, W_d, r_d, a_d or W, r_w, and a_w) we minimized the χ^2 function using the uncertainties of the elastic-scattering differential cross section. The resulting parameters from both seed sets, along with the values for the seed parameters, are given in Table I and denoted as FT (Trost seed calculated from the global formula [10]) and FVII (Vernotte family II seed taken from ^{18}O data [11]). In Fig. 2 the calculated angular distribution of ^{3}He using FT and FVII optical potentials is compared to the experimental data. Optical model parameters used for the exit channel are given in Table II. They were taken from Fulbright [12] or calculated from global formulas derived

TABLE I. Fit of optical model parameters in input channel ^{3}He + ^{15}N.

Pot.[a]	V (MeV)	r (fm)	a (fm)	W (MeV)	r_w (fm)	a_w (fm)	W_d (MeV)	r_d (fm)	a_d (fm)
Seed T	116.4	1.15	0.764	–	–	–	18.9	1.288	0.800
Fit FT	125.2	1.15	0.6870	–	–	–	11.3	1.4041	0.7469
Seed VII	183.5	1.15	0.659	7.9	2.142	0.695	–	–	–
Fit FVII	202.5	1.15	0.6074	11.4	1.7842	0.7918	–	–	–

[a]Seed T = parameters from Ref. [10]; FT = fit of our elastic scattering data; seed VII = parameter set II from Ref. [11]; FVII = fit of our elastic scattering data; $r_c = 1.4$ fm.

by Daehnick *et al.* [13]. The angular distributions for deuterons from the reaction ^{15}N(^{3}He, d)^{16}O corresponding to the eight bound states in ^{16}O calculated using the DWBA with different combinations of the optical model parameters are compared to the experimental data in Figs. 3 and 4.

IV. ASYMPTOTIC NORMALIZATION COEFFICIENTS

For the particle transfer reaction $A(a, b)B$, where $a = b + x$ and $B = A + x$, the DWBA cross section can be written [14] as

$$\frac{d\sigma}{d\Omega} = \left(C^B_{Axl_B j_B}\right)^2 \left(C^a_{bxl_a j_a}\right)^2 \frac{\tilde{\sigma}^{\text{DW}}_{l_B j_B l_a j_a}}{b^2_{Axl_B j_B} b^2_{bxl_a j_a}}, \quad (2)$$

where $\tilde{\sigma}^{\text{DW}}_{l_B j_B l_a j_a}$ is the reduced DWBA cross section, $C^a_{bxl_a j_a}$ and $C^B_{Axl_B j_B}$ are the projectile and final nucleus ANCs, j_i, l_i are the total and orbital angular momenta of the transferred particle in nucleus i, and the b's are the single-particle ANCs defining the amplitude of the tail of the radial single-particle bound-state wave functions. The projectile ANC corresponding to the vertex ^{3}He $\rightarrow d + p$ in the channel with $l_{^3\text{He}} = 0$ and $j_{^3\text{He}} = 1/2$, $(C^{^3\text{He}}_{\text{dp}})^2 = 3.90 \pm 0.06$ fm^{-1} was taken from Ref. [15].

The peripheral nature of the transfer reaction can be checked by different methods. A standard approach is to use the cutoff of the radial matrix element of the DWBA amplitude at small radii. The ratio in Eq. (3) offers an equivalent check of the peripheral nature of the transfer process. If the reaction is peripheral the dominant contribution to the reduced DWBA cross section comes from the region in the configuration space where the radial single-particle bound-state wave functions used in the DWBA calculations can be approximated by their tails, which implies $\tilde{\sigma}^{\text{DW(max)}}_{l_B j_B l_a j_a} \propto b^2_{Axl_B j_B} b^2_{bxl_a j_a}$. Then the ratio

$$R\left(b_{Axl_B j_B}, b_{bxl_a j_a}\right) = \frac{\tilde{\sigma}^{\text{DW(max)}}_{l_B j_B l_a j_a}}{b^2_{Axl_B j_B} b^2_{bxl_a j_a}}, \quad (3)$$

where $\tilde{\sigma}^{\text{DW(max)}}$ is the reduced DWBA differential cross section calculated at the main (first) maximum of the angular

distribution, is independent of the single particle ANCs $b_{Axl_B j_B}$ and $b_{bxl_a j_a}$ [14]. We checked the dependence of R on the single-particle ANC, $b_{Axl_B j_B}$, for the ^{16}O ground state, and one loosely bound excited state ($E_x = 10.957$ MeV). In Eq. (3) the reduced DWBA differential cross section was calculated at the main maximum of the angular distribution, which is the most forward (pronounced) peak in the transfer reaction and typically occurs at or near $0°$. In the vicinity of the main maximum, the transfer reaction is the most peripheral and a simple particle transfer mechanism (stripping) described by the DWBA gives the dominant contribution. Variation of the single-particle ANC b (for simplicity in what follows we drop the subscripts in the single-particle ANC b) can be achieved by changing the geometric parameters, radius r_0, and diffuseness a, of the Woods-Saxon bound state potential. The radius, r_0, was changed from 1.0 to 1.5 fm at fixed diffuseness of $a = 0.65$ fm. We calculated $R(b)$ using the combination of the optical potential sets of Trost *et al.* [10] and Fulbright *et al.* [12]. We find that the deviation of $R(b)$ from the central value calculated at $r_0 = 1.25$ fm for the transition to the ground state is about 3.5%. The deviation of $R(b)$ for transitions to excited states does not exceed 3.0%. Note that dependence of $R(b)$ on b also indicates the sensitivity of the determined ANCs to the choice of b.

According to Ref. [1] and our calculations shown in the next section only the ANC for the ground state is important for nuclear astrophysics. The DWBA calculations for the reaction ^{15}N(^{3}He, d)^{16}O populating the ground state of ^{16}O (see Fig. 3) agree very well with the experimental data within the main peak of the angular distribution. Normalizing the DBWA differential cross section to the experimental one in the main peak of the angular distribution [14] we determined the ANCs (Table III) for the ground and seven excited states of ^{16}O. From Table III we can infer the uncertainty of the ANCs for each state. The contributions are 10% experimental uncertainty (as explained in Sec. II), 9% due to the ambiguity of the optical potential parameters, and about 3% due to the residual dependence of the extracted ANCs on the bound-state potential parameters. The total uncertainty for the squares of the ANCs is about 14.5%. Although our primary goal

TABLE II. Parameters of the optical model potentials in the output channel d + ^{16}O.

Pot.	V (MeV)	r (fm)	a (fm)	W_d (MeV)	r_d (fm)	a_d (fm)	V_{so} (MeV)	r_{so} (fm)	a_{so} (fm)	r_c (fm)	Ref.
F	92	1.053	0.771	8.18	1.361	0.772	–	–	–	1.3	[12]
D	82.88	1.17	0.7478	11.74	1.325	0.5178	6.4	1.0700	0.660	1.3	[13]

TABLE III. ANCs from the ^{15}N(^{3}He, d)^{16}O reaction.

State (J^π)	(jl)	C^2_{Jjl}(fm^{-1})	SF[a] (our work)	SF[a] (Fulbright)[b]	SF[a] (Bohne1)[c]	SF[a] (Bohne2)[d]
g.s. (0^+)	(0.5, 1)	192.0 ± 26.0	2.10	1.76	1.30	1.33
6.1299(3^-)	(2.5, 2)	3.52 ± 0.44	0.39	0.32	0.36	0.40
6.9171(2^+)	(1.5, 1)	0.20 ± 0.06	0.009	–	0.01	0.01
7.1169(1^-)	(1.5, 0)	0.96 ± 0.12	0.20	0.27	0.21	0.20
8.8719(2^-)	(2.5, 2)	0.82 ± 0.12	0.30	0.28	0.44	0.36
9.8445(2^+)	(1.5, 1)	0.046 ± 0.010	0.006	–	–	–
10.957(0^-)	(0.5, 0)	13.6 ± 1.95	0.49	0.60	0.89	0.50
11.080(3^+)	(2.5, 3)	0.0010 ± 0.0002	0.05	–	0.09	–

[a]The SFs were determined for geometric parameters of the bound state potential $r_0 = 1.25$ fm and $a = 0.65$ fm.
[b]Reference [12].
[c]Reference [16].
[d]Reference [17].

is determination of the ANCs, in Table III we also present SFs calculated using equation SF = C^2/b^2 with b calculated for the bound-state potential parameters $r_0 = 1.25$ fm and $a = 0.65$ fm. Our SFs are compared with the ones reported in the literature. Although the determined ANCs are practically insensitive to the bound-state potential parameters, the SFs strongly depend on them. For example, for the ground state the variation of r_0 in the interval 1.0–1.5 fm at fixed a changes b^2 and, correspondingly, SF by a factor of 3.5. Hence, when presenting the SFs determined from different measurements the bound-state potential parameters also should be indicated. Our adopted ^{16}O bound-state potential parameters coincide with those given in Refs. [16,17]. Unfortunately no information is available about the bound-state parameters used in Ref. [12].

V. ASTROPHYSICAL FACTOR FOR ^{15}N(p, γ)^{16}O

We have calculated the S factor for this reaction using the two-channel, two-level R-matrix method. The contribution from the α-^{12}C channel is also taken into account. In the case
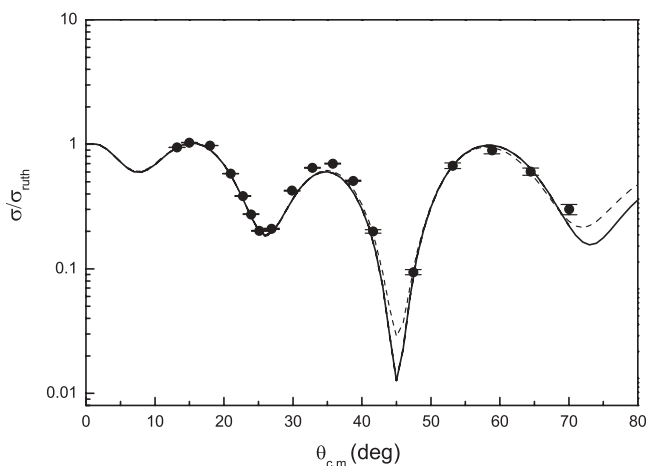

FIG. 2. The angular distribution of ^{3}He elastic scattering on ^{15}N obtained with the beam energy of 25.74 MeV. Curves represent final fits generated by optical potential sets FT (solid line) and FVII (dashed line) given in Table I.

under consideration, only two levels with $J^\pi = 1^-$ produce strong energy dependence corresponding to two resonances at 312 and 962 keV. If the channel radius is large enough, then the levels calculated for the Woods-Saxon potential will be close to the single-particle shell-model ones. The closest state to the subthreshold 1^- level is located at $E_x = 9.585$ MeV, but its ANC (or reduced width) is so small that we were not able to observe it. Hence we neglect this level. The other level at $E_x = 7.1169$ MeV is 5.06 MeV away from the threshold and also does not affect the behavior of the S factor at low energies. The levels located at higher energies can be included into the background [18], which has a very smooth energy dependence. The total reaction amplitude in the R-matrix approach for the capture to the ground state of ^{16}O (in the case of the interfering resonant and nonresonant terms) is

$$M(E) = i\Omega_p(E) \sum_{\nu,\lambda} A_{\nu\lambda}(E)[\Gamma_{\nu\gamma}(E)]^{1/2}\tilde{\Gamma}^{1/2}_{\lambda p}(E) + M^{\mathrm{NR}}(E).$$

(4)

Here, $\Omega_p(E)$ is the phase factor in the initial channel of the reaction, $\mathbf{A}(E)$ is the level matrix, $[\Gamma_{\nu\gamma}(E)]^{1/2}$ is the amplitude of the radiative width of the level ν decaying to the bound state, $\tilde{\Gamma}_{\lambda p}(E) = 2 P_l(E) \gamma_{\lambda p}$ is the formal proton width of the level λ, $\gamma_{\lambda p}$ is its reduced width, $P_l(E)$ is the barrier penetrability for protons, E is the relative energy in the channel p-^{15}N, and M^{NR} is the amplitude of the nonresonant radiative capture occurring in the external region.

In the two-level approximation $\lambda, \nu = 1, 2$, the resonant amplitude in Eq. (4) contains four terms rather than two terms used in Ref. [1]. It constitutes one of the differences between our fit and fit in Ref. [1]. We note that in the R-matrix method the nonresonant capture matrix element in the internal region does not explicitly appear. This nonresonant part is given by the radial integral taken from the channel radius r_0 to ∞ [3] and its absolute normalization is entirely determined by the ANC of the bound state [19]. Note that the ANC and the reduced width used in the R-matrix approach are related by Eq. (60) of Ref. [20].

The resonant parameters in Eq. (4) and channel radius are fitting parameters to reproduce the experimental data. We choose the channel radius in the proton channel to be $r_0 = $
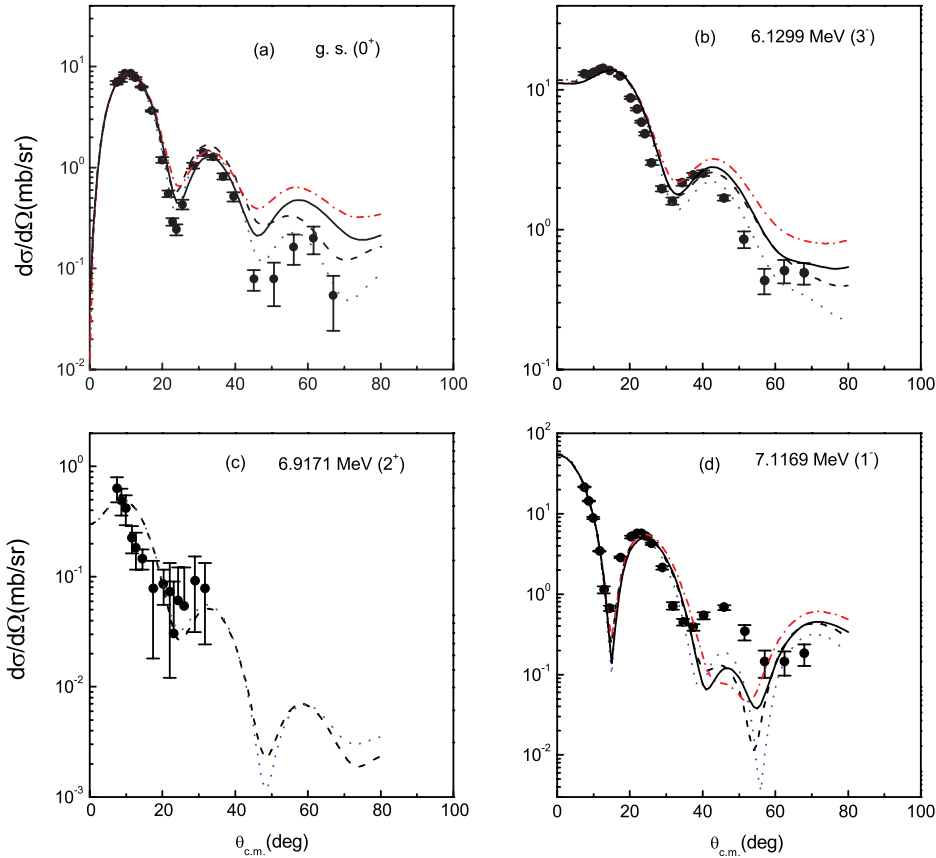
FIG. 3. (Color online) Angular distributions from the ^{15}N(^{3}He, d)^{16}O reaction for the transitions leading to the ground (a), 6.1299 MeV (b), 6.9171 MeV (c), and 7.1169 MeV (d) states in ^{16}O. DWBA calculations were performed with optical model parameter sets given in Tables I (input channel) and II (output channel): FVII-D, black solid curve; FT-F, black dashed curve; FVII-F, blue dotted curve; and FT-D, red dash-dotted curve.

5.0 fm. The proton and α reduced widths can be expressed in terms of the observable widths [18]. These widths are available in compilations [21]. But they are determined from different reactions with different uncertainties. First, we determined the proton and α reduced widths by fitting the measured astrophysical factor for the ^{15}N(p, α)^{12}C reaction in the R-matrix approach. In this fit the channel radii for the proton and α channels were taken to be 5.0 and 7.0, correspondingly. The search region for proton and α widths was originally taken from Ref. [21] and then extended for the α widths for the second resonance. Because the cross section for this reaction is significantly larger than for the ^{15}N(p, γ)^{16}O reaction, it has been measured with significantly higher accuracy. This allows us to determine the proton and α partial widths with higher accuracy. We used two different boundary conditions. First, we fixed the second level energy at $E_2 = E_{R_2} = 962$ keV, where E_{R_2} is the energy of the second resonance, and determined from the fit to the experimental data that the first level energy is $E_1 = 152$ keV. It means that in the R-matrix approach the two levels are separated by ≈ 800 keV. The χ^2 fit per degree of freedom is $\chi^2/N = 1.27$. If we adopt the first level energy to be $E_1 = E_{R_1} = 312$ keV, then the best fit is achieved for $E_2 = 1070$ keV with $\chi^2/N = 1.51$. The results of the fit are shown in Fig 5.

After determining the particle reduced widths, we made the R-matrix fit of the ^{15}N(p, γ)^{16}O data. To achieve a better fit for this reaction, we slightly readjusted the reduced widths. Both boundary conditions gave slightly different reduced widths and similar fits to the data. The main fitting parameters in this case are the complex radiative width amplitudes, $[\Gamma_{1\gamma}]^{1/2}$

and $[\Gamma_{2\gamma}]^{1/2}$. The radiative width amplitude consists of the internal and external (channel) parts [3]. The internal radiative width amplitude is real, whereas the external one is complex because the resonant scattering wave function in the external region is described by the outgoing wave. We find that the imaginary parts of the radiative width amplitudes are important for the fit of the experimental data. The best fit is achieved if we assume that the sign of the real parts of both radiative width amplitudes is the same and opposite to the sign of their imaginary parts. At fixed particle reduced widths the radiative width amplitudes determine the absolute value of the astrophysical S factor at the resonant peaks. According to [1] the S factors at the resonance peaks are 400 keV b. The absolute cross section was determined in Ref. [1] by normalization of the ^{15}N(p, $\alpha_1 \gamma_1$)^{12}C excitation function to the known cross section of $\sigma = 250 \pm 35$ mb at $E_R = 1134.40$ keV. Then from the observed relative intensity of γ rays from the ^{15}N(p, $\alpha_1 \gamma_1$)^{12}C and ^{15}N(p, γ_0)^{16}O reactions, the capture cross section for the latter reaction was determined. To determine accurately the uncertainty of the S factors at the resonance peaks one needs to know information, such as the errors of the measured γ-ray intensities and the uncertainty in the detector efficiency, which are not given in Ref. [1]. Thus we believe that a 14% uncertainty for the S factors at the resonance peaks is too optimistic. We assigned a 16% uncertainty to the S factors at the resonances from the $\approx 16\%$ uncertainties for the radiative widths for the first and second resonances given in Ref. [1]. We assigned a 16% uncertainty to the radiative widths of both resonances in our fit. The radiative widths obtained here by the normalization of the calculated
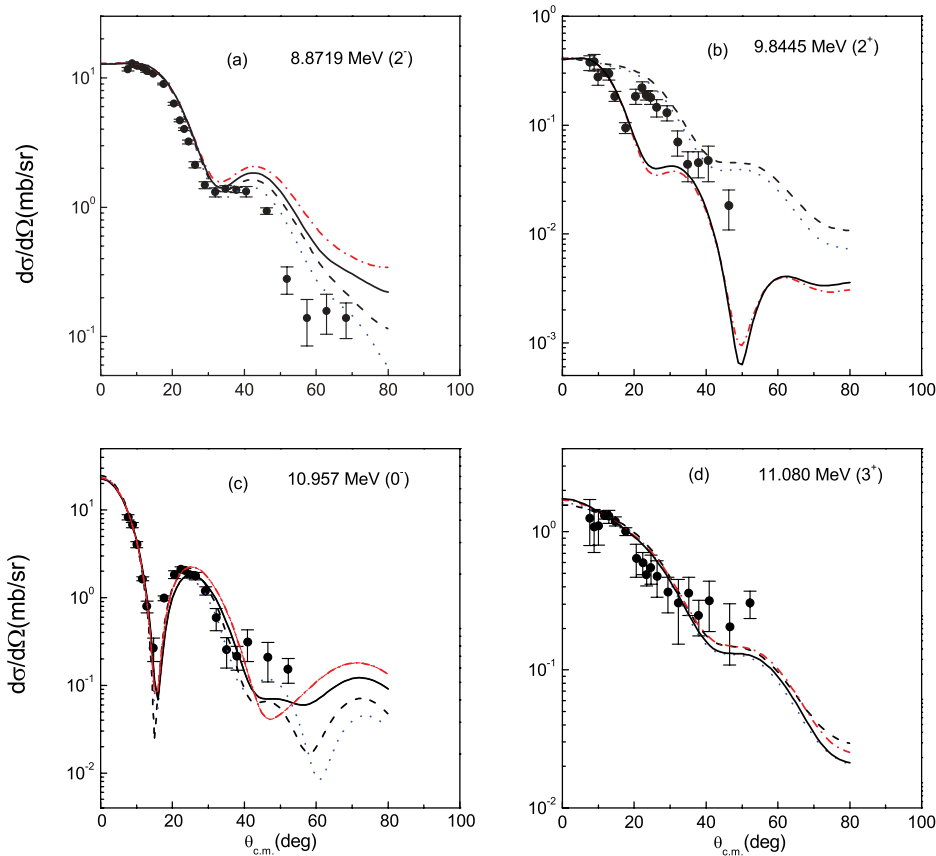
FIG. 4. (Color online) Angular distributions from the ^{15}N(^{3}He, d)^{16}O reaction for the transitions leading to the 8.8719 MeV (a), 9.8445 MeV (b), 10.957 MeV (c), and 11.080 MeV (d) states in ^{16}O. DWBA calculations were performed with optical model parameter sets given in Tables I (input channel) and II (output channel) for the transitions to the 8.8719 MeV (a), 10.957 MeV (c), and 11.080 MeV (d) states: FVII-D, black solid curve; FT-F, black dashed curve; FVII-F, blue dotted curve; and FT-D, red dash-dotted curve. For the transition to the 9.8445 MeV (b) state: FVII-F, black solid curve; FT-F, red dash-dotted curve (both for $1d_{3/2}$); FVII-F, blue dotted curve; and FT-F, black dashed curve (both for $1d_{5/2}$).

S factor to the experimental data are the ones are given in Table IV.

The χ^2 fit for the radiative capture is worse than for the (p, α) reaction because we are not able to reproduce the low-energy data from Ref. [1]. For the boundary condition
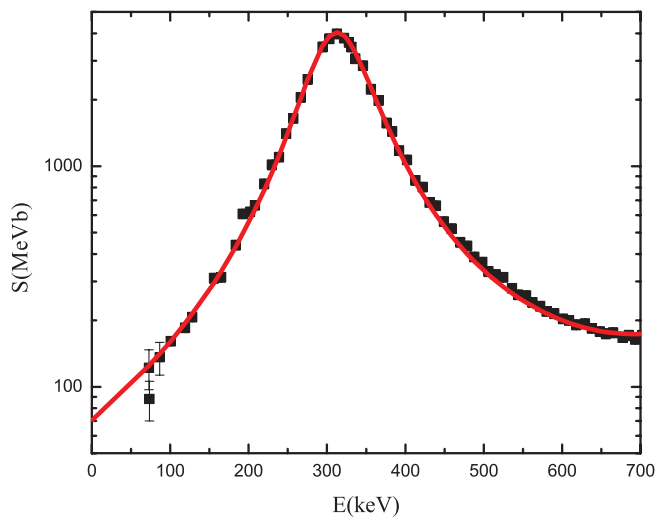

FIG. 5. (Color online) The astrophysical $S(E)$ factor for the ^{15}N(p, α)^{12}C reaction. The black squares are experimental data from Ref. [22]. The red solid line is our R-matrix fit with the boundary condition $E_2 = 962$ keV, which takes into account two interfering 1^- resonances at $E_{R_1} = 312$ and $E_{R_2} = 962$ keV.

$E_2 = E_{R_2} = 962$ keV we get $\chi^2/N = 2.8$ and for $E_1 = E_{R_1} = 312$ keV we get $\chi^2/N = 3.0$. The squares of the determined reduced widths for both boundary conditions are given in Table IV along with the reduced widths reported in Ref. [2]. We find that one of the α reduced widths (we cannot determine which one) has an opposite sign relative to three other particle reduced widths. In our fit we assumed that $\gamma_{1\alpha} < 0$. The level energies used in Ref. [2] are not given, which is why we cannot compare directly our parameters and the set from Ref. [2]. The observable widths of each resonance can be expressed in terms of the reduced widths when the corresponding level energy coincides with the resonance energy. From the R-matrix fit with the first level energy $E_1 = 312$ keV we get the observable partial widths for the first resonance, $\Gamma_{1p} = 1.1$ keV and $\Gamma_{1\alpha} = 90.5$ keV. From the R-matrix fit with the second level energy $E_2 = 962$ keV, we get the observable partial widths of the second resonance, $\Gamma_{2p} = 99.7$ keV b and $\Gamma_{2\alpha} = 50.4$ keV. The radiative widths are also given in Table IV. We note that our radiative width for the second resonance is higher than the reported value of $\Gamma_{2\gamma} = 32 \pm 5$ eV [1] but lower than $\Gamma_{2\gamma} = 88$ eV obtained in Ref. [2].

The two-channel, two-level R matrix fit to the experimental data for the S factor is shown in Fig. 6. The low-energy tail of our calculated S factor fitting the data from Ref. [2] goes along the lower limit of the data from Ref. [1]. Our astrophysical factor $S(0) = 36.0 \pm 6.0$ keV b obtained for the proton channel radius $r_0 = 5.0$ fm is lower then $S(0) = 64.0 \pm 6.0$ keV b [1] but agrees with $S(0) = 29.8 \pm$

TABLE IV. Resonance parameters.

Reference	γ_{1p}^2 (keV)	γ_{2p}^2 (keV)	$\gamma_{1\alpha}^2$ (keV)	$\gamma_{2\alpha}^2$	$\Gamma_{1\gamma}$ (eV)	$\Gamma_{2\gamma}$ (eV)
[2]	354	450	19.8	4.27	12.8	88
Present work ($E_1 = 312$ keV)	280.9	271.4	12.5	6.1	8.8 ± 1.5	–
Present work ($E_2 = 962.4$ keV)	407.0	270.4	9.6	6.1	–	50.0 ± 8.0

5.4 keV b [2] within uncertainties. We note that the R-matrix calculations show very little sensitivity to the variation of the channel radius r_0. Decreasing (increasing) r_0 increases (decreases) the integration region of the radial matrix element for the nonresonant capture, i.e., increases (decreases) the direct capture amplitude and decreases (increases) the resonant part, so the total sum remains nearly constant. A variation of the channel radius by 33% changes the $S(0)$ factor by 5%. The 17% uncertainty of our $S(0)$ astrophysical factor comes from the (assumed) 16% uncertainty of the experimental data, the 10% uncertainty of the ANCs, which results in about a 2% uncertainty in the $S(0)$ factor, and a 5% uncertainty due to the dependence of the S factor on the channel radius.

The most important difference between our fit and the result in Ref. [1] is in the contribution of the nonresonant capture to the ground state. The calculated S factor for the external nonresonant capture to the ground state, along with the total nonresonant S factor for captures to all observed bound states, is shown in Fig. 6. As we noted above, the absolute normalization of the nonresonant capture terms is entirely determined by the corresponding ANC in the R-matrix

approach. Because we have measured the ANCs, we can quite accurately determine the contribution from the nonresonant capture terms. At zero energy it contributes about 3.0% to the total astrophysical factor. But the nonresonant capture to the ground state, which contributes about 69% to the total nonresonant S factor, is much more important when calculating the total astrophysical factor due to its interference with the resonant capture terms. We find that our calculated nonresonant astrophysical factor for the capture to the ground state is $S(0) = 0.86$ keV b, i.e., about 9 times smaller than the $S(0)$ obtained in Ref. [1]. It is the main reason why our low-energy tail of the S factor goes lower than the data in Ref. [1]. Because normalization of the nonresonant capture amplitude is determined by the ANC, which has been determined with 10% uncertainty, we do not agree with the result obtained in Ref. [1] within the hard sphere approach. Unfortunately, there is no explanation of the method used to calculate the nonresonant capture terms in Ref. [1]. We note that we also tried to fit the ^{15}N$(p, \gamma)^{16}$O data using the expression given in Ref. [1] and failed to reproduce the low-energy tail of the S factor for the same reason.
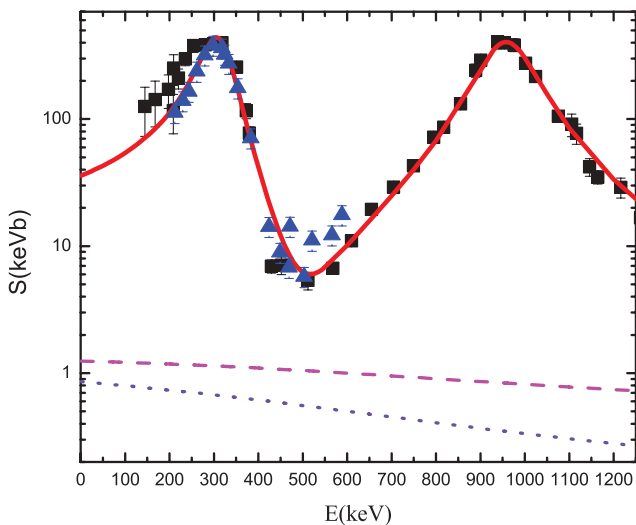

FIG. 6. (Color online) The astrophysical factor for the ^{15}N$(p, \gamma)^{16}$O reaction. The black squares are data from Ref. [1], the blue triangles are data from Ref. [2], the solid red line is our calculated $S(E)$ factor for the channel radius $r_0 = 5.0$ fm, the magenta dashed line is the total nonresonant capture S factor given by the sum of the nonresonant capture S factors to all eight bound states observed in the present ^{15}N$(^3$He, $d)^{16}$O experiment, and the violet dotted line is the nonresonant capture S factor to the ground state.

VI. SUMMARY AND CONCLUSION

The ^{15}N$(p, \gamma)^{16}$O reaction is an important astrophysical process, which provides a leak from the CN cycle into the CNO bi-cycle and CNO tri-cycle. It is contributed by the resonance capture to the ground state through two strong 1^- resonances and nonresonant capture to the ground state, which interferes with the resonant capture terms. To determine more accurately the contribution from the nonresonant captures we determined the proton ANCs for the ground and seven excited states of ^{16}O by measuring the angular distributions of the peripheral ^{15}N$(^3$He, $d)^{16}$O proton transfer reaction. To fit the available experimental astrophysical factors from Refs. [1,2] we determined the resonant proton and α partial widths by fitting the available experimental data for the stronger and better measured reaction ^{15}N$(p, \alpha)^{12}$C. Our astrophysical factor in the energy interval 150–300 keV agrees well with the data from Ref. [2] but goes slightly lower than the low limit of data reported in Ref. [1]. This new astrophysical factor, $S(0) = 36.0 \pm 6.0$ keV b, obtained for ^{15}N$(p, \gamma_0)^{16}$O allows us to re-evaluate the rate of leak from the CN cycle due to this reaction. In Ref. [1] it was estimated as the ratio of the $S(0)$ factors for ^{15}N$(p, \alpha)^{12}$C and ^{15}N$(p, \gamma_0)^{16}$O. The S factor $S(0) = 57$ MeVb was used for ^{15}N$(p, \alpha)^{12}$C. However, the later measurements [22] gave the higher value

of the astrophysical factor $S(0) = 65.0 \pm 4.0$ MeVb. Our new fit for the $^{15}N(p, \alpha)^{12}C$ data gives $S(0) = 71.0 \pm 5.0$ MeVb. This result overlaps, within the experimental uncertainties, with the S factor recently measured via the indirect Trojan horse method [24]. Using the data from Ref. [22] we can re-evaluate the loss of catalyst in the CN cycle at proton energy of 25 keV, which corresponds to the relative p-^{15}N energy $E = 23.44$ keV. We find, using our new astrophysical factor $S(E = 23.44\,\text{keV}) = 38.8 \pm 6.6$ keV b for the $^{15}N(p, \gamma_0)^{16}O$ reaction and 84.1 ± 5.9 MeVb for the $^{15}N(p, \alpha)^{12}C$ reaction, that for every 2200 ± 300 cycles of the main CN cycle one CN catalyst is lost due to the $^{15}N(p, \gamma_0)^{16}O$ reaction, rather than 1200 ± 100 cycles determined from data of Ref. [1] $S(E = 23.44\,\text{keV}) = 70.0 \pm 11.0$ keV b]. Our result agrees with the leak rate 2600 ± 400 cycles obtained with $S(E = 23.44\,\text{keV}) = 32.0 \pm 5.8$ keV b for the $^{15}N(p, \gamma_0)^{16}O$ reaction in Ref. [2].

Our calculated reaction rates for $^{15}N(p, \gamma_0)^{16}O$ for temperatures $T_9 < 0.15$ are lower than the adopted reaction rates given in the NACRE compilation by approximately a factor of 2 [25], which were calculated using data from Ref. [1]. We believe that, when new measurements of the astrophysical factor for $^{15}N(p, \gamma_0)^{16}O$ will be available, the reaction rates should be updated.

[1] C. Rolfs and W. S. Rodney, Nucl. Phys. **A235**, 450 (1974).

[2] D F. Hebbard, Nucl. Phys. **15**, 289 (1960).

[3] F. C. Barker and T. Kajino, Aust. J. Phys. **44**, 369 (1991).

[4] C. A. Gagliardi, R. E. Tribble, A. Azhari, H. L. Clark, Y.-W. Lui, A. M. Mukhamedzhanov, A. Sattarov, L. Trache, V. Burjan, J. Cejpek, V. Kroha, Š. Piskoř, and J. Vincour, Phys. Rev. C **59**, 1149 (1999).

[5] A. M. Mukhamedzhanov, P. Bém, B. A. Brown, V. Burjan, C. A. Gagliardi, V. Kroha, J. Novák, F. M. Nunes, Š. Piskoř, F. Pirlepesov, E. Šimečková, R. E. Tribble, and J. Vincour, Phys. Rev. C **67**, 065804 (2003).

[6] A. M. Mukhamedzhanov, P. Bém, V. Burjan, C. A. Gagliardi, B. F. Irgaziev, V. Kroha, J. Novák, Š. Piskoř, E. Šimečková, R. E. Tribble, F. Veselý, and J. Vincour, Phys. Rev. C **73**, 035806 (2006).

[7] D. R. Tilley, H. R. Weller, and C. M. Cheves, Nucl. Phys. **A564**, 1 (1993).

[8] P. D. Kunz, DWUCK5 code, http://spot.colorado.edu/kunz/DWBA.html.

[9] J. Raynal, ECIS79 code (unpublished).

[10] H. J. Trost, P. Lezoch, and U. Strohbusch, Nucl. Phys. **A462**, 333 (1987).

[11] J. Vernotte, G. Berrier-Ronsin, J. Kalifa, and R. Tamisier, Nucl. Phys. **A390**, 285 (1982).

[12] H. W. Fulbright, J. A. Robins, M. Blann, D. G. Fleming, and H. S. Plendl, Phys. Rev. **184**, 1068 (1969).

[13] W. W. Daehnick, J. D. Childs, and Z. Vrcelj, Phys. Rev. C **21**, 2253 (1980).

[14] A. M. Mukhamedzhanov, H. L. Clark, C. A. Gagliardi, Y.-W. Lui, L. Trache, R. E. Tribble, H. M. Xu, X. G. Zhou, V. Burjan, J. Cejpek, V. Kroha, and F. Carstoiu, Phys. Rev. C **56**, 1302 (1997).

[15] A. M. Mukhamedzhanov, R. E. Tribble, and N. K. Timofeyuk, Phys. Rev. C **51**, 3472 (1995).

[16] W. Bohne, H. Homeyer, H. Lettau, H. Morgenstern, J. Scheer, and F. Sichelschmidt, Nucl. Phys. **A128**, 537 (1969).

[17] W. Bohne, H. Homeyer, H. Lettau, H. Morgenstern, J. Scheer, and F. Sichelschmidt, Nucl. Phys. **A160**, 257 (1971).

[18] A. M. Lane and R. G. Thomas, Rev. Mod. Phys. **30**, 257 (1958).

[19] X. D. Tang, A. Azhari, C. A. Gagliardi, A. M. Mukhamedzhanov, F. Pirlepesov, L. Trache, R. E. Tribble, V. Burjan, V. Kroha, and F. Carstoiu, Phys. Rev. C **67**, 015804 (2003).

[20] A. M. Mukhamedzhanov and R. E. Tribble, Phys. Rev. C **59**, 3418 (1999).

[21] D. R. Tilley, H. R. Weller, and C. M. Cheves, Nucl. Phys. **A565**, 1 (1993).

[22] A. Redder *et al.*, Z. Phys. A **305**, 325 (1982).

[23] C. E. Rolfs and W. S. Rodney, *Cauldrons in the Cosmos* (The University of Chicago Press, Chicago, 1988).

[24] M. La Cognata, S. Romano, C. Spitaleri, S. Cherubini, V. Crucilla, M. Gulino, L. Lamia, R. G. Pizzone, A. Tumino, R. Tribble, Changbo Fu, V. Z. Goldberg, A. M. Mukhamedzhanov, D. Schmidt, G. Tabacaru, L. Trache, and B. F. Irgaziev, Phys. Rev. C **76**, 065804 (2007).

[25] C. Angulo *et al.*, Nucl. Phys. **A656**, 3 (1999).